Wall Interference Analysis by Whole Wind Tunnel CFD

Atsushi Hashimoto
Masataka Kohzai

Aerospace Research and Development Directorate
Japan Aerospace Exploration Agency
Chofu, Tokyo, 182-8522
JAPAN
ahashi@chofu.jaxa.jp

Abstract

For wall interference correction, the potential-based methods such as Mokry's method are commonly used. In fact, the linear correction methods cannot be used for transonic and stall conditions. In this study, the Mokry's method is applied to wind tunnel CFD, and the corrected aerodynamic coefficients are compared with CFD without wall to investigate validity and limitation of the method. We have simulated the whole wind tunnel flow of JAXA 2m×2m Transonic Wind Tunnel (JTWT). The pressure distribution on the wind tunnel wall agrees well with the measurements. In addition, the computed C_L and C_D agree well with the measured values. The differences between standard and long stings are almost same as the experiment. It is found that the aerodynamic characteristics of ONERA-M5 and its wall/support interferences are well reproduced in this computation. In the case of M=0.7, long sting, and $\alpha=0^{\circ}$, the results corrected by the Mokry's method show good agreement with those without wall. However, the accuracy is degenerated by shock wave, separation, and support interference, since the Mokry's method is based on the linear potential theory. It is found that the effect of support interference is not so large, whereas the effect of separation is serious.

Key words: Wind tunnel, CFD, Wall interference.

Introduction

Highly accurate aerodynamic data is required for development of civil aircrafts. For example, the requirement of drag forces measured at wind tunnel testing in the high-speed regime is ideally less than 1 count (1 count is 0.0001 of C_D). To achieve this severe accuracy requirement for force and moment measurements, the following techniques are important: flow quality maintenance, balance calibration, wall correction, and support correction. For JAXA 2m×2m transonic wind tunnel (JTWT), a series of activities to improve the measurement accuracy have been recently conducted; measurement of the flow angularity[1], calibration of test section Mach number[2], correction of thermal zero-shift of balance[3] and wall and support corrections[4].

For the wall correction, the potential-based methods such as Mokry's method[5] are commonly used. These correction methods are based on the small perturbation potential equation. Taking advantage of the linearity, the effect of wall interference can be extracted from the flow field in the wind tunnel. In fact, the linear correction methods cannot be used for transonic and stall conditions. However, the methods are widely used since the computation is simple and fast, and the accuracy is believed to be appropriate even under these conditions, although the methods are not strictly verified.

Recently, CFD especially RANS simulation is used for investigation of wall interference. ETW with slotted walls is directly simulated in Ref. 6. The guided far field model is also proposed to model the effect of ETW wall[7]. However, the verification of current wall correction method is rarely done with CFD, though the wind tunnel CFD considering the slotted or porous walls is commonly carried out. An example is the wall interference analysis of S2MA at ONERA[8]. The linear potential code DXV used for wall correction is validated with CFD results.

In this study, flow inside the JTWT is simulated to investigate the wall interferences under the transonic and stall conditions. The support effect on the wall interference is also investigated. The Mokry's method is applied to wind tunnel CFD, and the corrected aerodynamic coefficients are compared with CFD without wall. CFD is a powerful tool since it can simulate both conditions with and without wall, which is impossible by experiment.

Configuration of JTWT

The JTWT is a closed-circuit and continuously operating facility (Fig. 1). The wind tunnel has a square test section of 2m×2m. The JTWT can maintain the Mach number from 0.1 to 1.4 at the total pressure from 50 to 140 kPa.

An aircraft model installed in JTWT is shown in Fig. 2. We consider the ONERA-M5 wing-body model[16] as an aircraft model. The wing span is 0.9819m and the span to wind tunnel width ratio is 49%. The walls at the test section are porous ones. The support devices are sting, pod, and strut behind the model. In addition, there is a plenum chamber surrounding the test section. Here, we assume that the air is static and uniform in the plenum chamber.

In the computation, we consider a part of JTWT inside the red box in Fig. 1; nozzle, test section, and diffuser. Figure 3 shows the whole computational domain. The upstream converging nozzle region is also included to compute the growing turbulent boundary layer on the wind tunnel wall precisely. The diffuser behind the test section is also included in the computation to reduce the effect of outflow boundary. The closed-up figure of the test section is shown in Fig. 4. The ONERA-M5 model and the support devices (sting, pod, and strut) are included in the computation. The light-blue transparent walls in Fig. 4 are the porous walls. The windows in the side porous wall are also modeled precisely.

We employ two lengths of sting; standard and long stings shown in Fig. 5. The long sting is produced to investigate the buoyancy effects due to the support devices. The ONERA-M5 is located from STA=7409 to 8467 for standard sting and from STA=6968 to 8026 for long sting. The porous walls exist from STA=5200 to 9500.

Computational Methods

As a flow solver, the TAS (Tohoku University Aerodynamic Simulation) code[9] is used in this study. It is a well-validated code and used in a variety of aerospace applications[10]. In TAS, full Navier-Stokes equations are solved on the unstructured grid by a cell-vertex finite volume method. The HLLEW (Harten-Lax-van Leer-Einfeldt-Wada) method is used for the numerical flux computations. The LU-SGS (Lower/Upper Symmetric Gauss-Seidel) method is used for time integration. The second-order spatial accuracy is realized by a linear reconstruction of the primitive variables with Venkatakrishnan's limiter and Unstructured MUSCL-scheme (U-MUSCL). The Spalart-Allmaras model is used as a turbulence model and turbulent transition is not taken into account. The equations for the turbulence model are also solved using the second-order scheme. The time integration is carried out by the local time stepping. Since the wall interference is small, exactly same schemes must be used for all cases. Otherwise, the difference of scheme causes difference of aerodynamic forces and moments.

A grid is generated with MEGG3D[11]. The generated grid is a mixed element grid that consists of mainly tetrahedra and prismatic layers. The total number of node is 7.2 million for standard sting and 8.6 million for long sting. In this study, we compare results with and without wind tunnel walls to understand the wall interferences. To avoid the grid dependency, the exactly same surface grids are used for ONERA-M5, sting, pod, and strut. The grid resolution around the ONERA-M5 is almost same between the grids to be compared. We checked that the employed grids are sufficient to investigate the wall effects[15].

As for a porous wall model, a simple model developed by Nambu et al.[12,13] is employed. The model is developed specifically for JTWT conditions, where the hole geometry and thickness of turbulent boundary layer are considered. The mass flow rate through the porous wall is determined with this model from the pressure difference between the wind tunnel and the plenum chamber.

When we determine the velocity across the wall, at first, the pressure of plenum chamber is determined so that the mass inflow and outflow through the porous wall can be conserved. Here, we assume the pressure of plenum chamber is uniform. The computed velocity is set as boundary conditions of porous walls.

To realize the desired Mach number flow at the test section, the total pressure and temperature are fixed at the inflow boundary and the static pressure is adjusted at the outflow boundary. Additionally, we use the initial

conditions calculated with the quasi one-dimensional nozzle theory. Otherwise, the computation becomes unstable and the local time stepping is not applicable. The detail of computational method is described in Ref.14.

Computational Conditions

Mach numbers at the test section are 0.70 and 0.84. Reynolds numbers based on the mean aerodynamic chord of 137mm are 1.56×10^6 and 1.67×10^6 for M=0.70 and 0.84, respectively. The total pressure is 100kPa and the total temperature is 322K. The angle of attack is 0° for all cases.

We conduct five computational cases in Table 1 to reveal the wall and sting effects. Table 1 shows which components are included in the computation. The pod and strut are included with the standard or long sting.

Validation of Whole Wind Tunnel Simulation

Figure 6 shows Cp contour on the model and tunnel wall surfaces, where the upper and side porous walls are removed to see the inside of wind tunnel. We compare the pressure distribution on the porous wall with measurements along the three lines illustrated in Fig. 7: upper, lower, and side walls. In Fig. 8, the computed Cp distributions are compared with the measurements for M=0.7, $\alpha=0^\circ$, and long sting. The ONERA-M5 is located from STA=6968 to 8026 for long sting (Fig. 5(b)). The porous walls exist from STA=5200 to 9500. The results agree with the measurements for all walls. Especially, the location and variation of suction peak show good agreement with those of measurement on the upper wall. The pressure becomes low around the model on the upper and side walls due to the low pressure above the wing, whereas the pressure becomes high on the lower wall since the wall interferes with downwash flow coming from the model. Additionally, the pressure distribution on the side wall is affected by the window, since the wall around the window is not porous (Fig. 4). The other cases with different Mach numbers and sting lengths are compared with measurement and show good agreement with measurement as well[15]. The difference of Mach number and sting length is found to be well captured in these computations.

Tables 2 and 3 show aerodynamic data for M=0.7 and 0.84, respectively, where the C_L, C_D, and C_m are listed. The aerodynamic data are evaluated on the forward body excepting the base. The experimental data is corrected using the measured base and cavity pressures. The values of dC_L, dC_D, and dC_m in Tables 2 and 3 are the difference due to the sting length: "Long sting"-"Standard sting". Figures 9 and 10 are the comparison of C_L, C_D, and C_m between computation and experiment for the standard and long stings. Although the experiment data are obtained for attack angles from -5° to 2°, the computation is carried out only at 0° and 2° for the standard sting and 2° for the long sting.

As shown in Fig. 9 and 10, the computed C_L and C_D agree well with measurement, though Cm is a little higher. Moreover, the differences between standard and long stings are almost same as the experiment (Figs. 9-10 and Tables 2-3). The difference due to the sting length is large in the drag force CD.

Validation of wall correction method

We apply the Mokry's method to the wind tunnel CFD to investigate validity and limitation of the method. The following steps are carried out to validate the method.

1. Implement wind tunnel CFD under the original conditions (M, α). ("Standard sting + Wall" or "Long sting + Wall" in Table 1)
2. Probe the wall pressure distribution of CFD result.
3. Calculate the correction values (ΔM, $\Delta\alpha$) from the wall pressure using the Mokry's method.
4. Correct the aerodynamic coefficients using ΔM and $\Delta\alpha$.
5. Implement CFD without wall under the corrected conditions ($M+\Delta M$, $\alpha+\Delta\alpha$). (e.g. "Standard sting" or "Long sting" in Table 1)

Here, we compare the results of step 4 and 5 for the cases in Table 4, where the original and corrected values are shown. If the aerodynamic coefficients of step 4 and 5 are same, the Mokry's method is found to be valid. Shock waves exist for M=0.84, whereas they do not exist for M=0.70. In addition, the flow is largely separated at the leading edge for $\alpha=2^\circ$, whereas it is separated behind the shock wave for $\alpha=0^\circ$.

Figures 11-13 show C_D, C_L, and C_m data for M=0.70 and 0.80 with the standard and long stings. These figures show uncorrected and corrected aerodynamic coefficients (e.g. "CFD Standard Support" and "CFD

Standard Support Corrected" in Fig. 11). The uncorrected data are obtained by the wind tunnel CFD. These coefficients are corrected with the Mokry's method using the wall pressure distribution of wind tunnel CFD. Moreover, the coefficients are computed again without wall under the corrected conditions (e.g. "CFD Standard Support w/o wall" in Fig. 11). If the results without wall agree with the corrected values, the Mokry's method is validated. Experimental data are also shown as a reference. The experimental data are adjusted to match the uncorrected CFD data at $\alpha=0^{\circ}$ in Figs 11 and 13, at $\alpha=2^{\circ}$ in Fig 12 to see the relative displacement.

As a whole, the corrected values of CFD are almost same as those of experiment, since the wall pressure is almost same between experiment and CFD as shown in Fig. 8. The case of M=0.7, long sting, and $\alpha=0^{\circ}$ shows the best agreement among them (Fig. 13) since this condition is adequate for potential-based methods. There is no shock wave, separation, and the support interference is small in this case. We mention these effects on the Mokry's method as follows, comparing this case with another case.

The difference between M=0.7 and 0.84 in Fig.13 is caused by the shock wave. Drag and pitching moment are not corrected accurately. In addition, Figs. 14-15 show the surface Cp and difference between uncorrected wind tunnel CFD and corrected CFD without wall for M=0.7 and 0.84, respectively. The difference is so small for M=0.7 (Fig. 14), whereas the pressure is different around the shock wave for M=0.84 (Fig. 15). It is found that the shock location is not corrected accurately with this method.

The difference between the standard and long stings (Figs.11 and 13) is caused by support interference. The differences are not large especially for M=0.7. The pitching moment becomes better for M=0.84 with standard support interference than that of long support. In fact, the pressure distribution on the wind tunnel wall is affected by the support interference. Although the empty pressure gradient (the buoyancy effect) is removed when the wall pressure is used for Mokry's method, these results indicate that the nonlinear interference between ONERA-M5 and support is not removed perfectly. Figure 16 show the Cp contour in the case of the standard sting, M=0.7. The difference is as small as that of the long sting (Fig. 11).

The difference between the attack angles of 0° and 2° (Figs.11 and 12) is caused by the separated flow around the wing tip. This difference is rather large, compared with the effects of shock wave and support interference. All coefficients of C_D, C_L, and C_m are not corrected accurately. The Cp contour for attack angle of 2°, M=0.7 are shown in Fig. 17. The difference is large at the separation region around the wing tip.

Finally, the summary of results is shown in Table 5. The accuracy is degenerated by shock wave, separation, and support interference. It is found that the effect of support interference is not so large, whereas the effect of separation is serious.

Conclusions

We have simulated the whole wind tunnel flow of JAXA 2m×2m Transonic Wind Tunnel (JTWT) to investigate wall interference and its correction method. The Mokry's method is applied to wind tunnel CFD, and the corrected aerodynamic coefficients are compared with CFD without wall.

The pressure distribution on the wind tunnel agrees well with the measurements. Therefore, the corrected aerodynamic coefficients of CFD are almost same as those of experiment. In addition, the computed C_L and C_D agree well with the measured values, though Cm is a little higher. The differences between standard and long stings are almost same as the experiment. It is found that the aerodynamic characteristics of ONERA-M5 and its wall/support interferences are simulated accurately.

In the case of M=0.7, long sting, and $\alpha=0^{\circ}$, the results corrected by the Mokry's method show good agreement with those without wall. However, the accuracy is degenerated by shock wave, separation, and support interference, since the Mokry's method is based on the linear potential theory. The effect of support interference is not so large, whereas the effect of separation is serious. The limitation of the method becomes clear in this study.

Acknowledgement

The authors would like to thank Mr. Kentaro Tanaka and Mr. Tohru Hirai of Ryoyu System Co., Ltd. for their computational support, Dr. Kazuomi Yamamoto, Dr. Mitsuhiro Murayama, Dr. Norikazu Sudani, Mr. Makoto Ueno, and Dr. Takashi Aoyama of JAXA for useful discussion, and Mr. Taisuke Nambu of Waseda University for the porous wall modeling.

References

[1] Ueno, M., Sudani, N., "Flow Angularity Measurement of 2m×2m Transonic Wind Tunnel," AIAA paper 2008-849, 2008.

[2] Kohzai, M., Ueno, M., Shiohara, T., Sudani, N., "Calibration of the test section Mach number in the JAXA 2m×2m Transonic Wind Tunnel," AIAA 2008-848, 2008.

[3] Kohzai, M., Shiohara, T., Ueno, M., Komatsu, Y., Karasawa, T., Koike, A., Sudani, N., Gahana, Y., Ikeda, M., Watanabe, A., Haraguchi, T., Nakagawa, M., Udagawa, D., "Thermal Zero Shift Correction of Strain-Gage Balance Output in the JAXA 2m×2m Transonic Wind Tunnel," JAXA Research and Development Report, JAXA-RR-07-034E, 2008.

[4] Kohzai, M., Sudani, N., Yamamoto, K., Ueno, M., Hashimoto, A., "Experimental and Numerical Studies of Support Interference in the JAXA 2m×2m Transonic Wind Tunnel," AIAA paper 2010-4200, 2010.

[5] Mokry, M., "Subsonic Wall Interference Corrections for Finite-Length Test Sections Using Boundary Pressure Measurements," Proceedings of the Fluid Dynamics Panel Specialists' Meeting, 1982, pp.10.1-10.5, AGARD CP-335.

[6] Bosnyakova, S., Kursakova, I., Lysenkova, A., Matyasha, S., Mikhailova, S., Vlasenkoa, V., Quest, J., "Computational Tools for Supporting The Testing of Civil Aircraft Configurations in Wind Tunnels," Progress in Aerospace Sciences, 44, 2008, pp. 67–120.

[7] Heidebrecht, A., "Simulation and model support correction for slotted wall transonic wind tunnels," 47th International Symposium of Applied Aerodynamics, 2012.

[8] Hantrais-Gervois, J.-L., Mouton, S. and Piat, J.-F., "RANS simulations to compute wind tunnel wall corrections," 47th International Symposium of Applied Aerodynamics, 2012.

[9] Nakahashi, K., Ito, Y., Togashi, F., "Some challenges of realistic flow simulations by unstructured grid CFD," *International Journal for Numerical Methods in Fluids*, Vol.43, pp.769-783, 2003.

[10] Murayama, M. and Yamamoto, K., "Comparison Study of Drag Prediction by Structured and Unstructured Mesh Method," *Journal of Aircraft*, Vol.45, No.3, 2008, pp. 799-822.

[11] Ito, Y., Shih, A., Soni, B. K., "Unstructured Mesh Generation Using MEGG3D - Mixed-Element Grid Generator in Three Dimensions," Proceedings of the International Conference on Numerical Geometry, Grid Generation and Scientific Computing (NUMGRID2008), Moscow, Russia, June 2008, pp. 5-11.

[12] Nambu, T., Hashimoto, A., Aoyama, T., Sato, T., "Analysis and Modeling of Flow through wind tunnel porous wall", AIAA paper 2010-4858, 2010.

[13] Nambu, T., Hashimoto, A., Murakami, K., Sato, T., "Numerical Analysis of Wind Tunnel Wall Interference on Two-dimensional Airfoil by New Porous Wall Model," AIAA paper 2012-3229, 2012.

[14] Hashimoto, A., Aoyama, T., Kohzai, M., Yamamoto, K., "Transonic Wind Tunnel Simulation with Porous Wall and Support Devices," AIAA paper 2010-4201, 2010.

[15] Hashimoto, A., Kohzai, M., Takashi, A., and Murayama, M., "Wall Interference Analysis of Transonic Wind Tunnel with Porous Wall Model," AIAA paper 2011-3017, 2011.

[16] Second Aerodynamics Division, National Aerospace Laboratory (NAL), "Results of the Test on ONERA Calibration Model M5 in NAL 2m×2m Transonic Wind Tunnel," NAL-TR-774T, 1983, Japan.

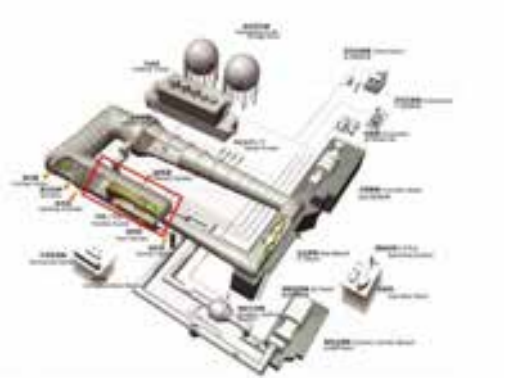

Figure 1 JAXA 2m×2m Transonic Wind Tunnel

Figure 2 ONERA-M5 model installed in JTWT

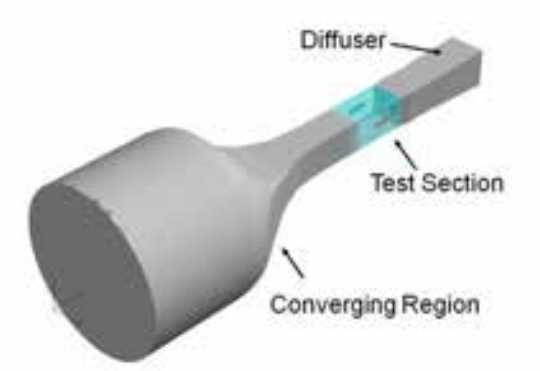

Figure 3 Whole computational domain

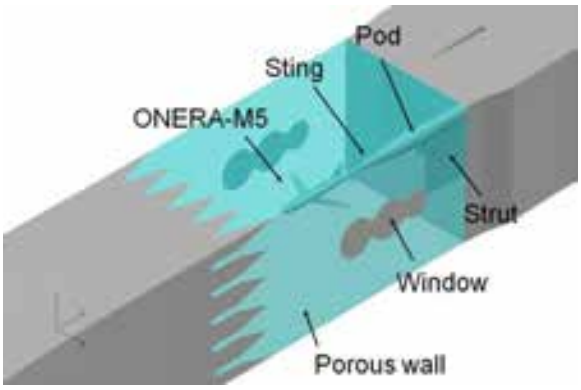

Figure 4 Closed-up view of test section

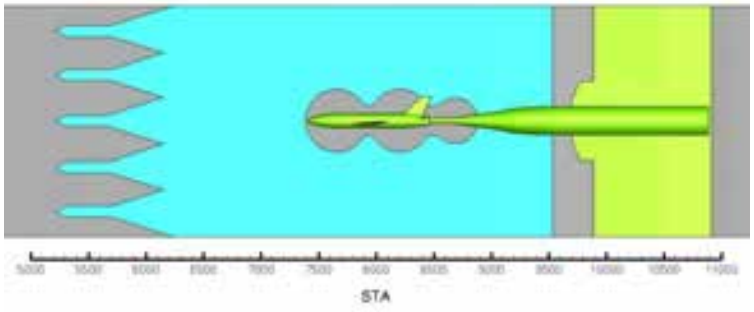

(a) Standard sting

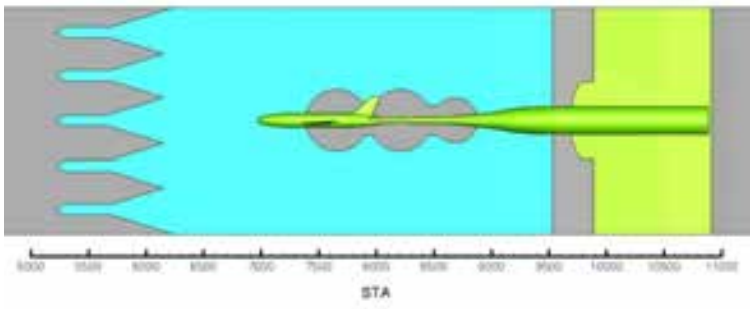

(b) Long sting

Figure 5 two types of sting

Table 1 Computational cases

Name	M5	Standard sting	Long sting	Pod	Strut	Wall
M5 Only	✓					
Standard sting + Wall	✓	✓		✓	✓	✓
Standard sting	✓	✓		✓	✓	
Long sting + Wall	✓		✓	✓	✓	✓
Long sting	✓		✓	✓	✓	

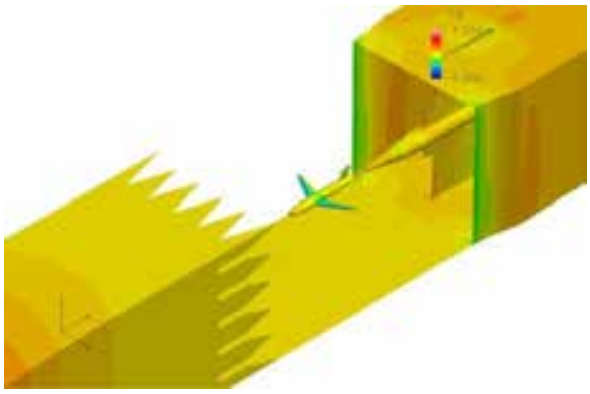

Figure 6 Cp contour

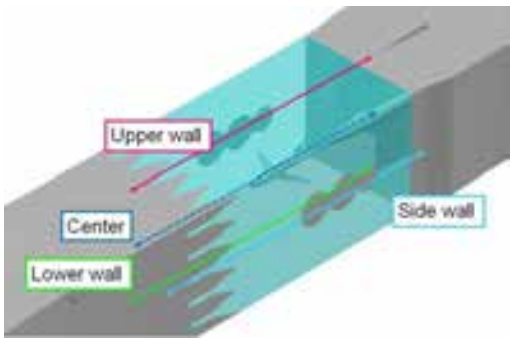

Figure 7 Line locations

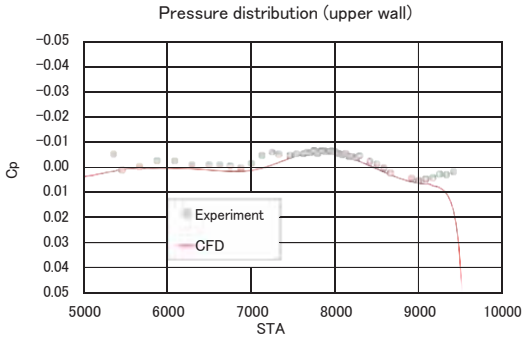

(a) Pressure distribution on the upper wall

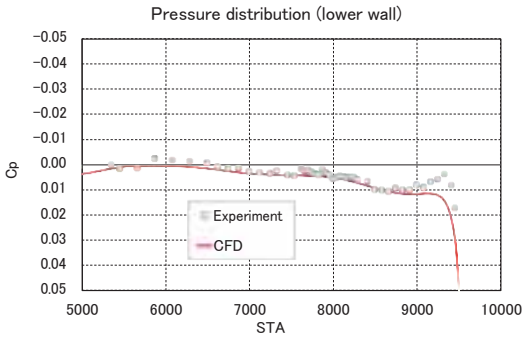

(b) Pressure distribution on the lower wall

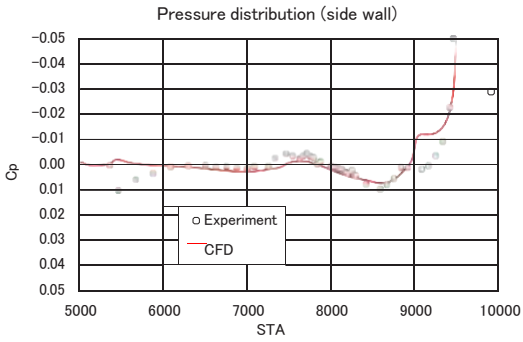

(c) Pressure distribution on the lower wall

Figure 8 Comparison of pressure on the porous wall (M=0.70, Long sting case)

Table 2 Aerodynamic data for M=0.7, α=0°, standard and long stings

	CL	CD	Cm	dCL	dCD	dCm	
Long Sting + Wall	0.307	0.0302	0.083	0.000	0.0010	0.003	"Long Sting + Wall"−"Standard Sting + Wall"
Standard Sting + Wall	0.307	0.0292	0.080				
Long Sting	0.311	0.0301	0.083	0.001	0.0012	0.003	"Long Sting"−"Standard Sting"
Standard Sting	0.309	0.0290	0.080				
M5 Only	0.309	0.0327	0.082				
Long Sting + Wall (EXP)	0.306	0.0304	0.078	−0.002	0.0010	0.004	"Long Sting + Wall(EXP)"−"Standard Sting + Wall(EXP)"
Standard Sting + Wall (EXP)	0.309	0.0293	0.075				

Table 3 Aerodynamic data for M=0.84, α=0°, standard and long stings

	CL	CD	Cm	dCL	dCD	dCm	
Long Sting + Wall	0.368	0.0437	0.092	−0.001	0.0018	0.005	"Long Sting + Wall"−"Standard Sting + Wall"
Standard Sting + Wall	0.369	0.0419	0.088				
Long Sting	0.376	0.0437	0.091	0.001	0.0018	0.003	"Long Sting"−"Standard Sting"
Standard Sting	0.375	0.0419	0.088				
M5 Only	0.377	0.0460	0.091				
Long Sting + Wall (EXP)	0.359	0.0424	0.083	−0.004	0.0014	0.004	"Long Sting + Wall(EXP)"−"Standard Sting + Wall(EXP)"
Standard Sting + Wall (EXP)	0.363	0.0410	0.079				

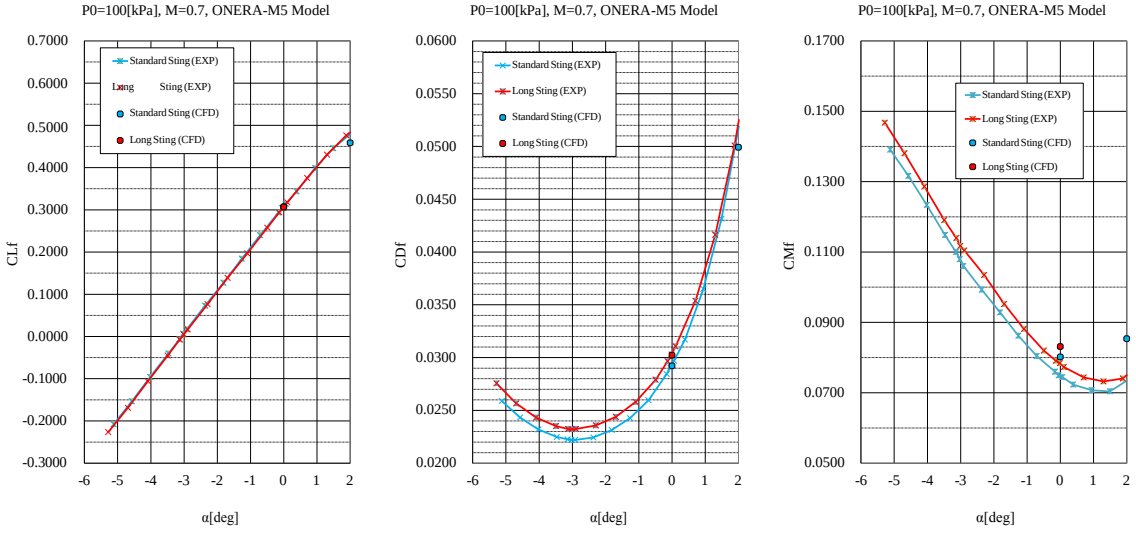

(a) C_L-α (b) C_D-α (c) C_m-α

Figure 9 Comparison of forces with experiment data (M=0.7, standard and long sting)

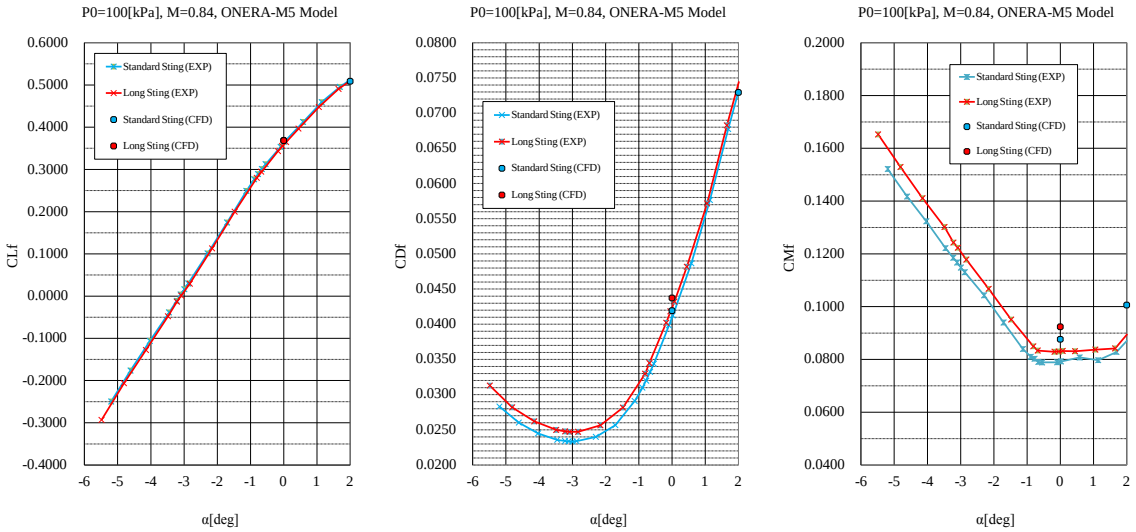

(a) C_L-α (b) C_D-α (c) C_m-α

Figure 10 Comparison of forces with experiment data (M=0.84, standard and long stings)

Table 4 Conditions corrected by Mokry's method

	Original		Corrected	
	M	Alpha (deg)	M	Alpha (deg)
Standard sting	0.70	0	0.699	-0.04
	0.70	2	0.699	1.95
	0.84	0	0.839	-0.07
	0.84	2	0.838	1.91
Long sting	0.70	0	0.700	-0.04
	0.84	0	0.839	-0.07

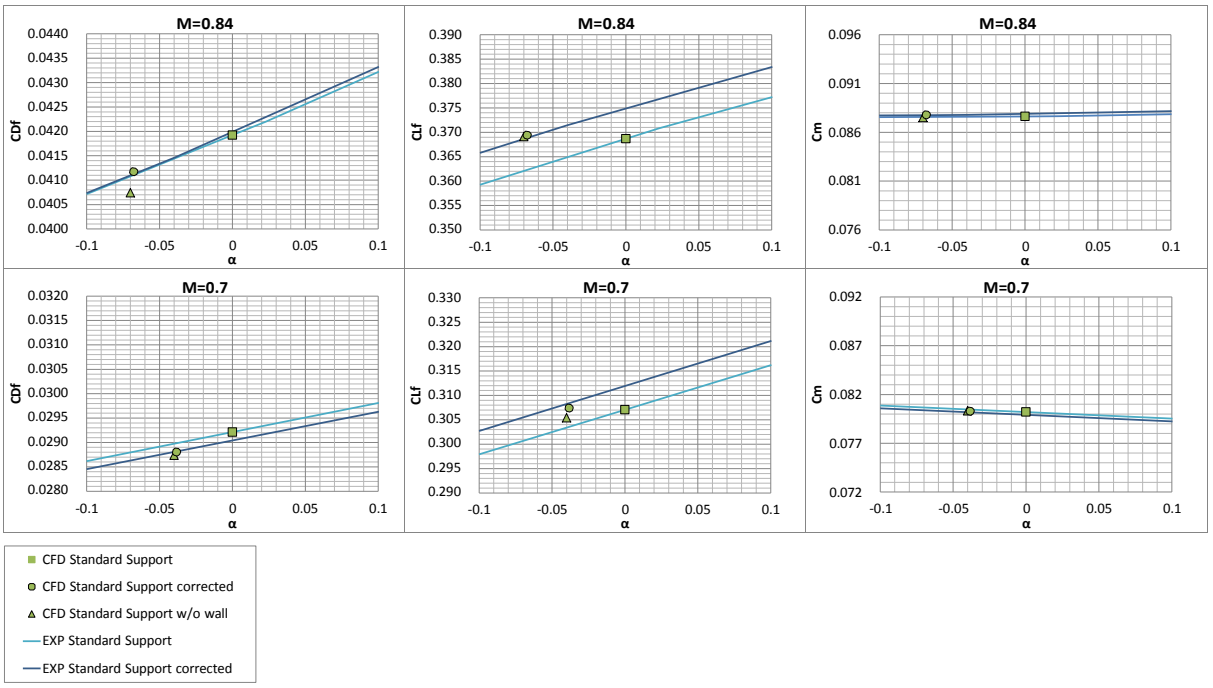

Figure 11 Corrected force and moment (Standard sting, α=0°)

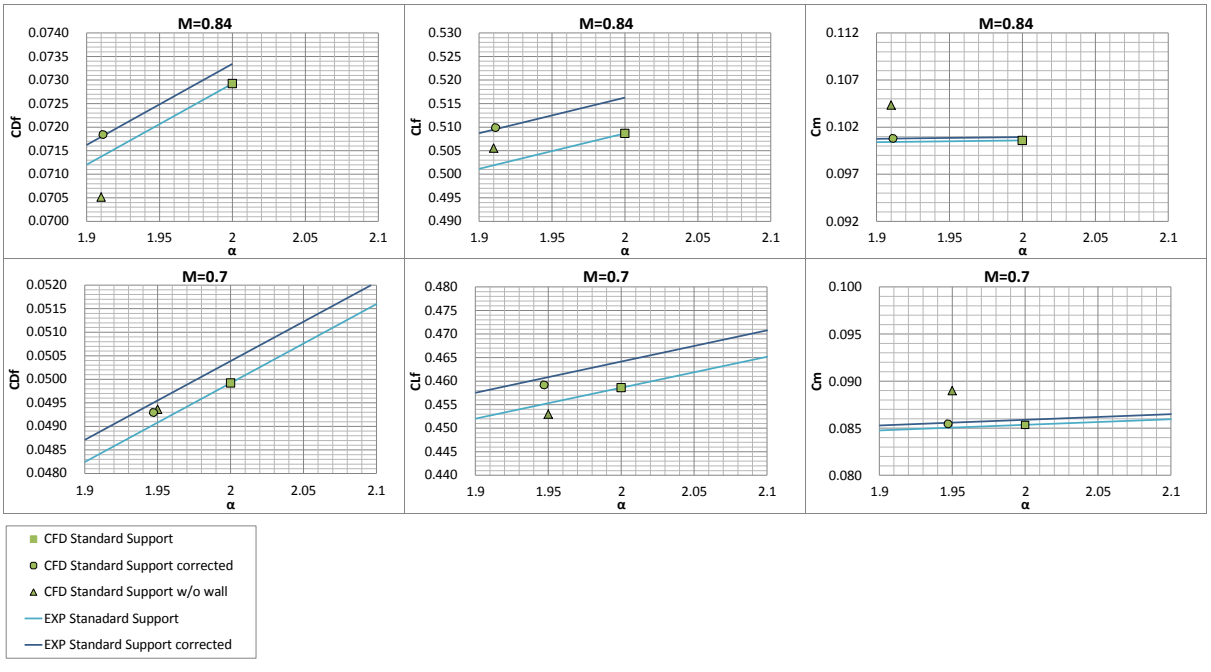

Figure 12 Corrected force and moment (Standard sting, α=2°)

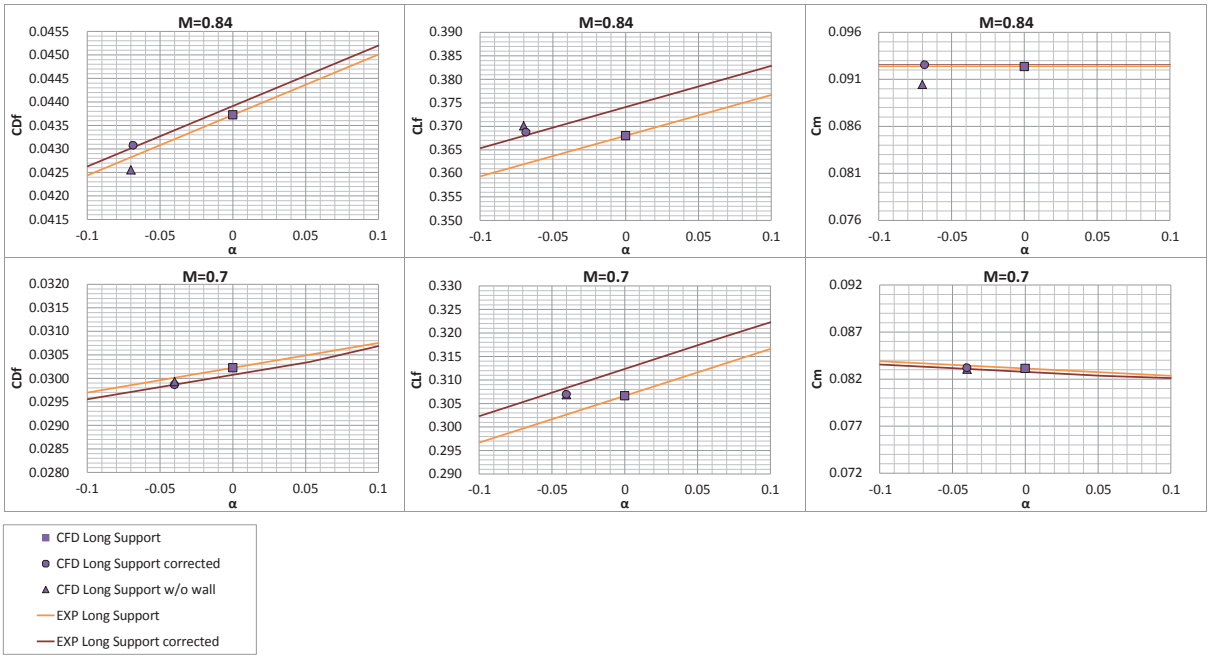

Figure 13 Corrected force and moment (Long sting, α=0°)

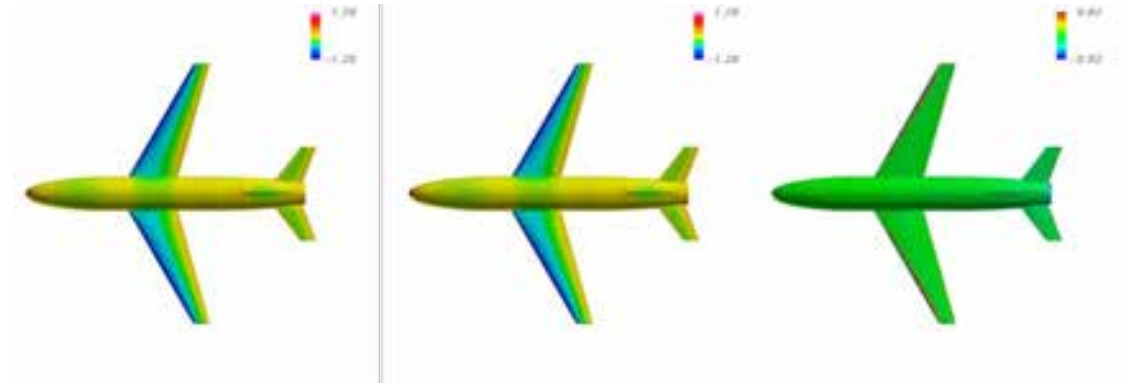

(a) With wall (original condition) (b) Without wall (corrected condition) (c) difference

Figure 14 Surface Cp contour (M=0.7, Long sting, α=0°)

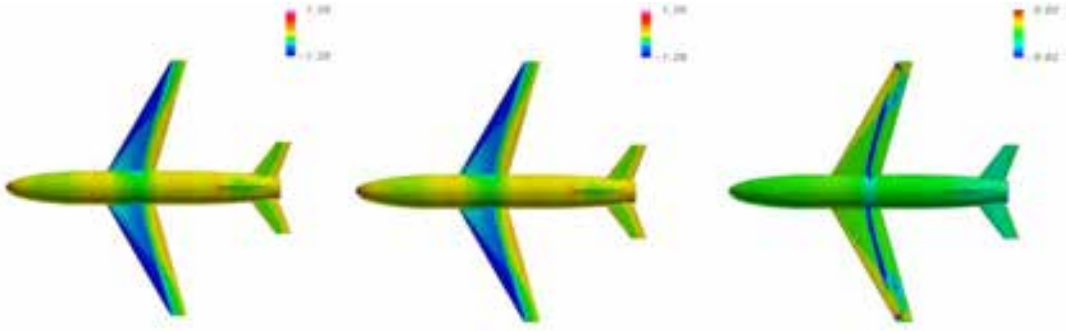

(a) With wall (original condition) (b) Without wall (corrected condition) (c) difference

Figure 15 Surface Cp contour (M=0.84, Long sting, α=0°)

(a) With wall (original condition) (b) Without wall (corrected condition) (c) difference

Figure 16 Surface Cp contour (M=0.7, Standard sting, α=0°)

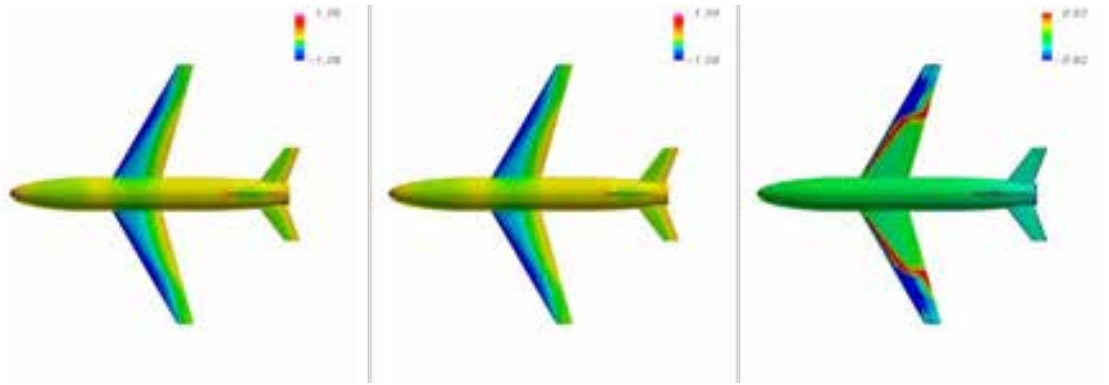

(a) With wall (original condition) (b) Without wall (corrected condition) (c) difference

Figure 17 Surface Cp contour (M=0.7, Standard sting, α=2°)

Table 5 Validation summary of Mokry's wall correction method

Sting	Mach	Attack angle	Shock wave	Separation	Support Interference	Mokry's method
Standard	0.7	0			✓	Good
Standard	0.84	0	✓	✓ (Small)	✓	Good
Standard	0.7	2		✓ (Large)	✓	Bad
Standard	0.84	2	✓	✓ (Large)	✓	Bad
Long	0.7	0				Excellent
Long	0.84	0	✓	✓ (Small)		Poor